(Received 13 October 2023, Accepted 28 December 2023, Scheduled 9 January 2024)

Compact and Broadband CPW-to-RWG Transition Using Resonator with Impedance-Matching Element

Ir-Ving Tseng, Ming-Feng Zheng, Ting-Tzu Cho*, and Chun-Long Wang

National Taiwan University of Science and Technology, Taipei 106335, Taiwan

ABSTRACT: This paper proposes a compact and broadband coplanar waveguide (CPW)-to-rectangular waveguide (RWG) transition using a resonator with an impedance-matching element. The transition size is as small as 7.66 mm, and the frequency range for which the reflection coefficient is smaller than −15 dB covers from 8.05 GHz to 12.18 GHz (FBW = 40.83%), almost encompassing the full X-band (8.2–12.4 GHz). To reduce the size of the transition, a short-circuited stub phase shifter is used to replace the half-wavelength phase shifter, resulting in a miniaturized CPW-to-RWG transition using the resonator with the impedance-matching element. The transition size is further reduced from 7.7 mm to 5.9 mm. Besides, the frequency range for which the reflection coefficient is smaller than −15 dB covers from 8.05 GHz to 12.38 GHz (FBW = 42.38%), nearly encompassing the full X-band (8.2–12.4 GHz) as usual. To verify the simulation results, both CPW-to-RWG transitions using the resonator with the impedance-matching element are fabricated and measured. The simulation and measurement results are in reasonable agreement.

1. INTRODUCTION

Due to the emerging development of the low earth orbit (LEO) satellite system, rectangular waveguide (RWG) has regained the academy's interest since the RWG can provide lowloss and high-power components, which the LEO system demands. On the other hand, planar transmission lines, invented in the 1960s, are commonly used in modern microwave systems due to their salient features of low cost, easy fabrication, lightweight, and easy integration with active components. Among planar transmission lines, coplanar waveguide (CPW) prevails in printed circuit board (PCB) layout since all its metals are on the same surface of the PCB, facilitating the shunt interconnection of the surface mount devices (SMDs). To integrate the systems realized by CPW and RWG, a CPW-to-RWG transition is required.

Various types of broadband CPW-to-RWG transitions have been proposed in the literature [1–13]. Since 1990, ridge waveguide has been used to accomplish broadband CPW-to-RWG transitions [1–5]. However, the size of the ride waveguide is large, and the mechanical process used to fabricate the ridge waveguide is complicated, increasing the transition cost. To tackle the complex fabrication process of the ridge waveguide, CPW-to-RWG transitions using the planar type transitions are proposed [6–13]. First, a broadband CPW-to-RWG transition using the fin-line taper is presented [6]. However, the size of the tapered fin-line is pretty extensive, consisting of several quarter-wavelengths. To reduce the size of the transition, broadband CPW-to-RWG transitions using one quarter-wavelength tapered slotline probe are proposed [7, 8]. However, these transitions require an additional intermediate transition, which adds to the size of these transitions.

To eliminate the intermediate transition, a broadband CPW-to-RWG transition using a quarter-wavelength horizontal probe is proposed [9]. Although there is no need for an intermediate transition, a significant substrate overhead is required. To eliminate the substrate overhead, a broadband CPW-to-RWG transition using a bow-tie antenna is proposed [10]. However, the size of the bow-tie antenna is approximately a half-wavelength, which is twice that of the quarter-wavelength. To reduce the size of the transition, a compact CPW-to-RWG transition using the quarter-wavelength dipole slot antenna is proposed [11]. However, the bandwidth is reduced. To enhance the bandwidth, a compact and broadband CPW-to-RWG transition using the quarter-wavelength stub resonators is proposed [12]. Since there is no need for the intermediate transition and substrate overhead, the transition size is as tiny as a quarter-wavelength. Besides, a broadband WR4-band CPW-to-RWG transition using the interdigital-pin EBG structure is proposed [13]. However, the size would be increased over a quarter-wavelength.

To reduce the circuit size further, a CPW-to-RWG transition using a resonator with an impedance-matching element is proposed. Properly designing the dimensions of the resonator and the impedance-matching element allows the transition size to be substantially reduced while the broadband response can be maintained.

2. COMPACT AND BROADBAND CPW-TO-RWG TRANSITION USING RESONATOR WITH IMPEDANCE-MATCHING ELEMENT

2.1. Topology

The schematic view of the CPW-to-RWG transition using a resonator with an impedance-matching element is depicted in Fig. 1(a) along with its planar view shown in Fig. 1(b) where the

* Corresponding author: Ting-Tzu Cho (tzcho3654@gmail.com).

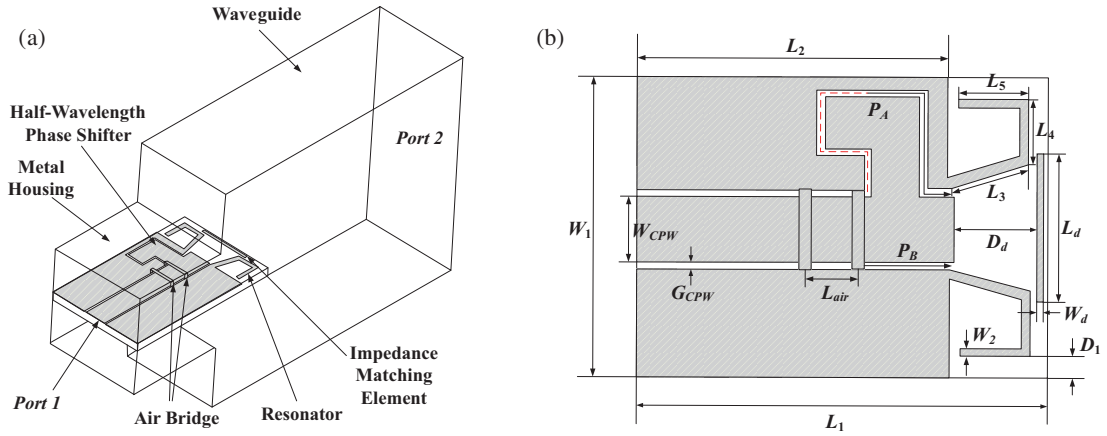

FIGURE 1. Schematic view of the CPW-to-RWG transition using the resonator with the impedance matching element. (a) 3-D view. (b) Planar view.

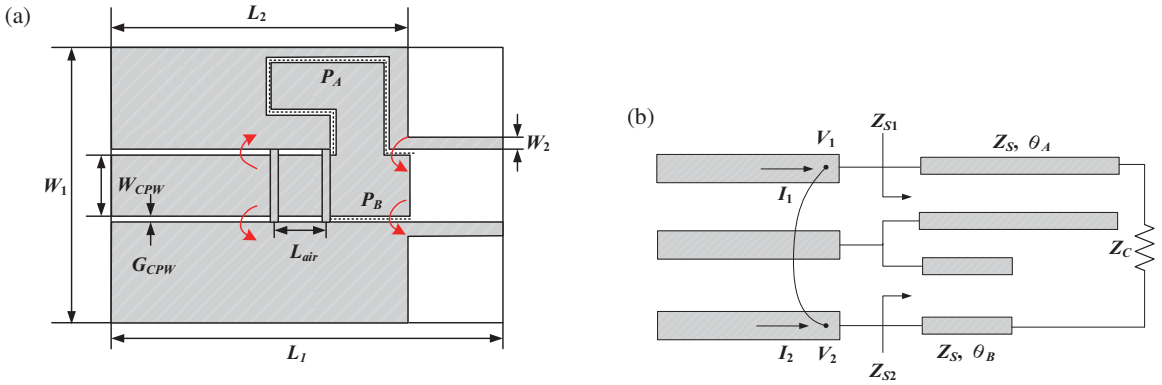

FIGURE 2. The half-wavelength phase shifter. (a) Layout. (b) Equivalent circuit.

areas with the slanted lines represent the metal part of the planar circuit. As can be seen from Fig. 1(a), the planar circuit consists of the feed-in CPW, a half-wavelength phase shifter, and a resonator with the impedance-matching element, which are implemented on a Rogers® RO4003C substrate with a relative dielectric constant of 3.55 and a thickness of 0.8 mm. The rectangular waveguide used here is a standard X-band (8.2–12.4 GHz) WG-90 waveguide, which ensures only TE_{10} mode propagation in X-band.

The feed-in CPW, which has a characteristic impedance of 50 Ω, is packaged within a metal housing to prevent the CPW from mechanical damage and electromagnetic interference from the outside environment. The cross-sectional dimensions of the housing are chosen as $10.16 \times 10.16\,\text{mm}^2$ so that there would be no waveguide modes propagating in the housing within the X-band. Consequently, the CPW mode will not be disturbed by the waveguide modes of the metal housing. To successfully convert the CPW mode into coupled slotline (CSL) mode, a phase shifter with 180° phase shifts is required. The air bridges are used to equal the potential of the CPW grounds, eliminating the backward reflection of the CSL mode into the CPW feed-in and therefore, enhancing the CSL mode's forward propagation into the resonator with the impedance-matching element. Eventually, the electric field of the CSL mode would be fed into the resonator with the impedance-matching element and coupled to the TE_{10} mode of the RWG.

2.2. Half-Wavelength Phase Shifter

Reconsidering Fig. 1(b), the design procedure of the transition would start with the determination of the half-wavelength phase shifter shown in Fig. 2(a). The complete response of the transition would be accomplished by including the influence of the resonator and impedance-matching element. Considering Fig. 2(a), since the characteristic impedance of the CPW is 50 Ω, the corresponding strip width W_{CPW} and slot width G_{CPW} of the CPW are determined to be 2.6 mm and 0.2 mm, respectively, using the Linecalc. As the slot width $G_{CPW} = 0.2$ mm is selected, the corresponding characteristic impedance of the slotlines Z_S is calculated to be 90 Ω. Given the coplanar strip width $W_2 = 0.4$ mm along with the coplanar slot width $W_{CPW} + 2G_{CPW} = 3$ mm, the characteristic impedance of the coplanar strip Z_C is calculated to be 281 Ω.

To facilitate the design procedure, Fig. 2(a) is represented with its ideal transmission line model shown in Fig. 2(b), where θ_A and θ_B represent the electrical lengths of the two slotlines; Z_S represents the characteristic impedance of the two slotlines; Z_{S1} and Z_{S2} represent the input impedances of the slotlines; Z_C represents the characteristic impedance of the coplanar strip. By comparing Fig. 2(a) and Fig. 2(b), it can be seen that the air bridge is approximated by a short circuit, and the discontinuity effects of the right-angled bend of the slotlines are ignored in the equivalent circuit of the half-wavelength phase

shifter shown in Fig. 2(b). These effects would be accounted for later.

Reconsidering Fig. 2(b), to transfer the CPW mode into CSL mode, a 180° phase shifter is required. As a result,

$$\theta_A(f_0) - \theta_B(f_0) = \pi \tag{1}$$

should be satisfied where f_0 represents the center frequency of the phase shifter. Since the characteristic impedance of the coplanar strip Z_C is equal to 281 Ω, which is large compared to the characteristic impedance of the CPW, the coplanar strip port could be approximated with an open circuit. As a result, the input impedances of the slotlines can be described by

$$Z_{S1} = -jZ_S \cot\theta_A(f) \tag{2}$$

$$Z_{S2} = -jZ_S \cot\theta_B(f) \tag{3}$$

As can be seen from Fig. 2(b), the voltages and currents could be related by

$$V_1 = Z_{S1} \times I_1 \tag{4}$$

$$V_2 = Z_{S2} \times I_2 \tag{5}$$

Since the air bridges connect the two ground planes of the CPW, the voltages V_1 and V_2 should be equal as

$$V_1 = V_2 \tag{6}$$

The input impedance Z_{in} of the CPW is defined as

$$Z_{in} = \frac{V_1}{I_1 + I_2} \tag{7}$$

By substituting (2), (3), (4), (5), and (6) into (7), the input impedance Z_{in} of the CPW could be rewritten as

$$Z_{in} = \frac{-jZ_s \cot\theta_A(f)\cot\theta_B(f)}{\cot\theta_A(f) + \cot\theta_B(f)} \tag{8}$$

As can be observed from (8), when the electrical lengths of the slotlines satisfy the following equation

$$\theta_A(f_r) + \theta_B(f_r) = n\pi, \quad n = 1, 2, 3, \tag{9}$$

at the resonance frequency $f = f_r$, the denominator of (8) would become zero, as shown below

$$\begin{aligned} &\cot\theta_A(f_r) + \cot\theta_B(f_r) \\ =\ &\cot[n\pi - \theta_B(f_r)] + \cot\theta_B(f_r) = 0 \end{aligned} \tag{10}$$

As a result, the input impedance Z_{in} in (8) would be $Z_{in} = \infty$, and resonance happens. This resonance frequency should be located out of the transition band to spare the transition performance. By comparing (9) with (1), the lowest value of n in (9) should be 2. As a result, the lowest resonance frequency f_r should satisfy the following equation

$$\theta_A(f_r) + \theta_B(f_r) = 2\pi \tag{11}$$

where the relationships between the electrical length $\theta_A(f_r)$ and $\theta_B(f_r)$ at the resonance frequency f_r and the electrical lengths $\theta_A(f_0)$ and $\theta_B(f_0)$ at the center frequency f_0 are related by

$$\theta_A(f_r) = \frac{f_r}{f_0}\theta_A(f_0) \tag{12}$$

$$\theta_B(f_r) = \frac{f_r}{f_0}\theta_B(f_0) \tag{13}$$

By substituting (12) and (13) into (11), we have the following equation.

$$\frac{f_r}{f_0}\theta_A(f_0) + \frac{f_r}{f_0}\theta_B(f_0) = 2\pi \tag{14}$$

Equations (1) and (14) can be used to determine the electrical lengths of the two slotlines, given the values of the center frequency f_0 and the resonance frequency f_r. The center frequency f_0 is chosen to be 10.3 GHz, which is the center frequency of the X-band (8.2–12.4 GHz). The inevitable resonance frequency f_r is determined to be 12.4 GHz, which is placed outside of the desired X-band. Given the center frequency $f_0 = 10.3$ GHz and the resonance frequency $f_r = 12.4$ GHz, the electrical lengths of the two slotlines are calculated to be $\theta_A = 240°$ and $\theta_B = 60°$ at $f_0 = 10.3$ GHz using (1) and (14).

To verify the resonance frequency of the equivalent circuit shown in Fig. 2(b), the commercial software ADS is used to simulate the equivalent circuit with $\theta_A = 240°$, $\theta_B = 60°$, and $Z_C = 281\,\Omega$. The frequency response of the reflection coefficient is shown in Fig. 3. As can be seen from Fig. 3, there is a peak in the frequency response of the reflection coefficient at 12.4 GHz, which is expected by the results of (1) and (14). To account for the parasitic effects of the air bridges and the discontinuity effects of the right-angled slotlines, Fig. 2(b) is implemented with the half-wavelength phase shifter shown in Fig. 2(a). The path lengths of the slotlines P_A and P_B are calculated to be 11.56 mm and 2.9 mm, respectively. The air-bridges' width, height, and distance are 0.3 mm, 0.4 mm, and 1.9 mm, respectively. Fig. 2(a) and path lengths $P_A = 11.56$ mm and $P_B = 2.9$ mm are simulated using the commercial software Ansoft® HFSS. The frequency response of the reflection coefficient is also shown in Fig. 3. As can be seen from Fig. 3, the resonance frequency f_r of the layout resides at 12.4 GHz, which is the same as the resonance frequency f_r of the equivalent circuit.

2.3. Resonator and Impedance-Matching Element

As can be seen from Fig. 3, although the half-wavelength phase shifter has already been designed in the X-band, the level of the reflection coefficient is around −10 dB. To reduce the level of the reflection coefficient, the characteristic impedance of the coplanar strip should be matched to the output impedance of the half-wavelength phase shifter shown in Fig. 1(b). The impedance-matching could be accomplished by adequately choosing the dimensions of the resonator and impedance-matching element. The length L_r of the resonator is determined to be 7 mm to set the matching frequency dip at 8.9 GHz, around the lower edge of the X-band. The width W_d of the impedance-matching element is set as 0.3 mm, which has negligible influence on the transition performance. The length L_d of the impedance-matching element is set equal to 5.2 mm, which will produce a matching frequency dip at 11.8 GHz. The distance D_d is set to be 2.9 mm away from the ground plane,

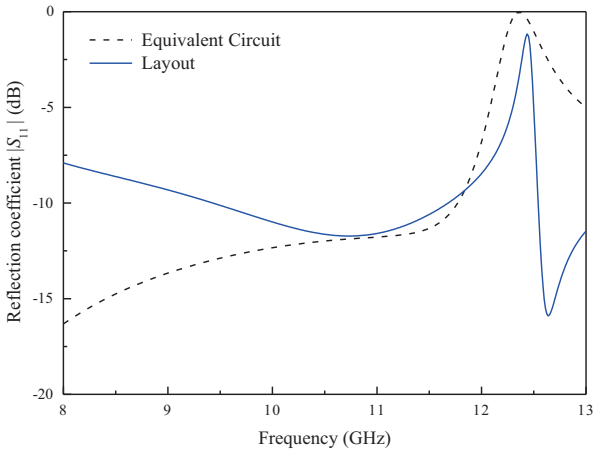

FIGURE 3. The frequency responses of the reflection coefficients $|S_{11}|$ for the equivalent circuit and layout of the half-wavelength phase shifter.

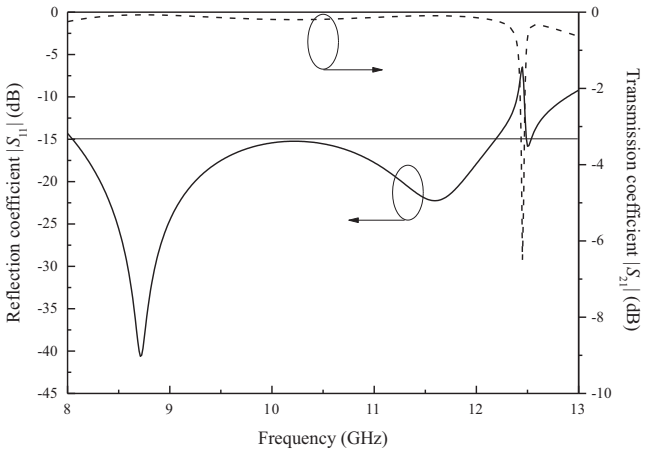

FIGURE 4. The frequency responses of the reflection coefficient $|S_{11}|$ and transmission coefficient $|S_{21}|$ for the CPW-to-RWG transition using the resonator with the impedance matching element.

FIGURE 5. Measurement setup for the back-to-back CPW-to-RWG transition using the resonator with the impedance matching element.

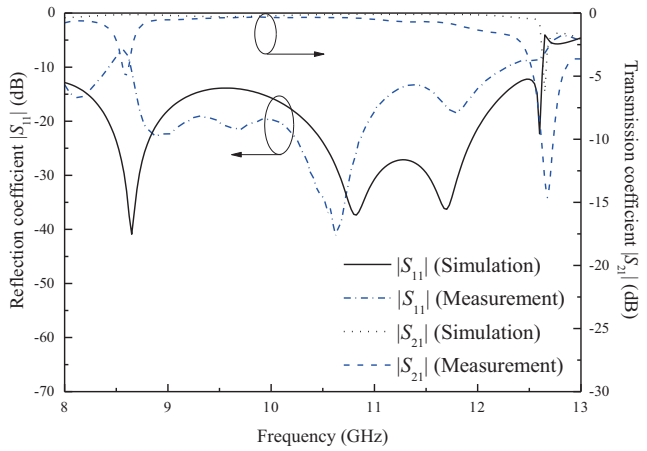

FIGURE 6. Comparison between the simulation and measurement results for the back-to-back CPW-to-RWG transition using the resonator with the impedance matching element.

which is limited by the fabrication tolerance of the gap 0.15 mm between the resonator and impedance-matching element.

Table 1 summaries the dimensions of the CPW-to-RWG transition using the resonator with the impedance-matching element shown in Fig. 1(b). As can be seen from Table 1, the length of the resonator with the impedance-matching element is 3.3 mm, which is much smaller than the length of a quarter-wavelength. The overall size of the transition is as small as 7.66 mm. Fig. 1(b) along with the dimensions listed in Table 1 is simulated by using the Ansoft HFSS, and the frequency responses of the reflection and transmission coefficients are shown in Fig. 4. As can be seen from Fig. 4, the bandwidth, for which the reflection coefficient is smaller than -15 dB, covers from 8.05 GHz to 12.18 GHz, almost encompassing the whole X-band (8.2–12.4 GHz), and the corresponding transmission coefficient in this frequency range is larger than -0.22 dB.

TABLE 1. Dimensions of the CPW-to-RWG transition using the resonator with the impedance matching element.

UNIT: mm

W_1	W_{CPW}	W_d	W_2	L_1	L_2	L_3	L_4
10.16	2.6	0.4	0.4	16.5	13.05	3	2.35
L_5	L_d	D_1	D_d	G_{CPW}	L_{air}	P_A	P_B
2.5	5.2	0.6	2.9	0.2	1.9	11.56	2.9

2.4. Verification

To verify the simulation results of the CPW-to-RWG transition using the resonator with the impedance-matching element shown in Fig. 1, two CPW-to-RWG transitions using the resonator with the impedance-matching element are back-to-back cascaded and fabricated as shown in Fig. 5. Fig. 5 is then measured by using the Agilent E8363B PNA after the network ana-

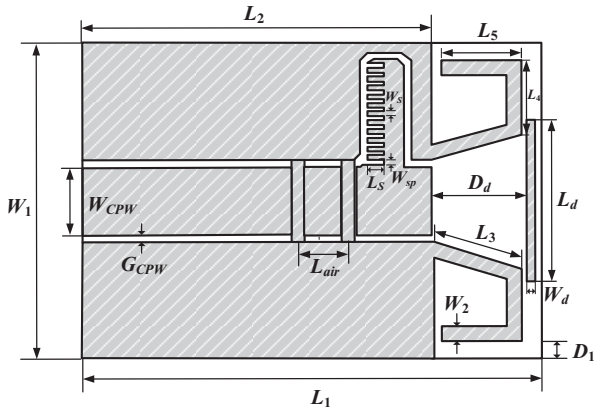

FIGURE 7. Planar view of the miniaturized CPW-to-RWG transition using the resonator with the impedance matching element.

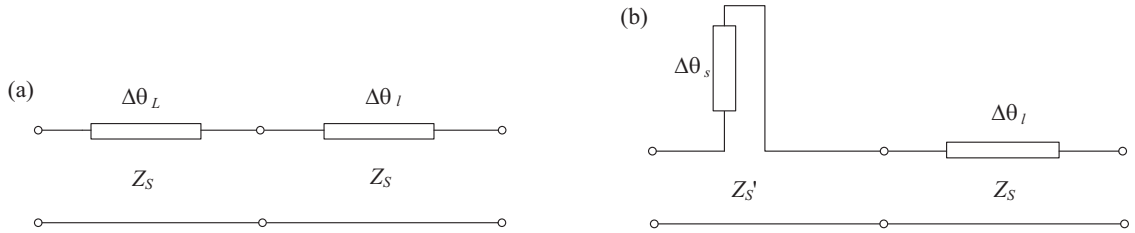

FIGURE 8. Equivalent circuit of the short-circuited stub. (a) Unit section model. (b) Short-circuited stub model.

lyzer is calibrated with the SOLT waveguide components. The measured frequency responses of the reflection and transmission coefficients are shown in Fig. 6, along with the simulated frequency responses of the reflection and transmission coefficients for the back-to-back transition. As shown in Fig. 6, the simulation and measurement results are in reasonable agreement except for some deviations, which the PCB fabrication process may cause.

3. MINIATURIZED CPW-TO-RWG TRANSITION USING RESONATOR WITH IMPEDANCE-MATCHING ELEMENT

3.1. Topology

To miniaturize the size of the CPW-to-RWG transition using the resonator with the impedance-matching element shown in Fig. 1(b), a short-circuited stub phase shifter is used to replace the half-wavelength phase shifter. The schematic view of the miniaturized CPW-to-RWG transition using the resonator with the impedance-matching element is shown in Fig. 7.

3.2. Short-Circuited Stub Phase Shifter

To miniaturize the size of the half-wavelength phase shifter shown in Fig. 1(b), the lower part of path A is selected (dashed line) and miniaturized through the technique of the short-circuited stub. The selected part of path A, which is denoted by an electrical length θ, is divided into N unit sections, and one unit section is characterized by an electrical length $\Delta\theta$ as shown in Fig. 8(a). The unit section can be further divided into two subsections, which are denoted by the electrical lengths $\Delta\theta_L$ and $\Delta\theta_l$. When the electrical length $\Delta\theta_L$ is small and the characteristic impedance of the slotline Z_S relatively large, this subsection $\Delta\theta_L$ can be replaced by a short-circuited stub with an electrical length $\Delta\theta_s$ as shown in Fig. 8(b). The relationship between the electrical length $\Delta\theta_L$ and electrical length $\Delta\theta_s$ can be derived by matching the phases of the transmission coefficients of these two components as shown in (15)

$$Z'_s \tan(\Delta\theta_s) = 2Z_s \tan(\Delta\theta_L) \tag{15}$$

In this case, the electrical length θ of the selected part of path A is $\theta = 73°$ at the center frequency $f_0 = 10.3$ GHz. This selected part of path A is divided into $N = 9$ sections with each unit section possessing an electrical length of $\Delta\theta = 8.11°$. The unit section is then divided into two subsections for which the electrical lengths of $\Delta\theta_L$ and $\Delta\theta_l$ are chosen as 5.92° and 2.19°, respectively. Given $Z_S = 90\,\Omega$, $Z'_S = 85\,\Omega$, and $\Delta\theta_L = 5.92°$, the value of the electrical length $\Delta\theta_s$ can be calculated to be 12.4° through using (15). To verify the equivalence between the unit section model shown in Fig. 8(a) and the short-circuited stub model shown in Fig. 8(b), Fig. 8(a) and Fig. 8(b) are simulated by using the commercial software Agilent ADS, and the frequency responses of the phases of the transmission coefficients S_{21} for these two models are shown in Fig. 9. As can be seen from Fig. 9, the phases of the transmission coefficients of these two models are in good agreement, which demonstrates that it is reasonable to replace the unit section model shown in Fig. 8(a) with the short-circuited stub model shown in Fig. 8(b).

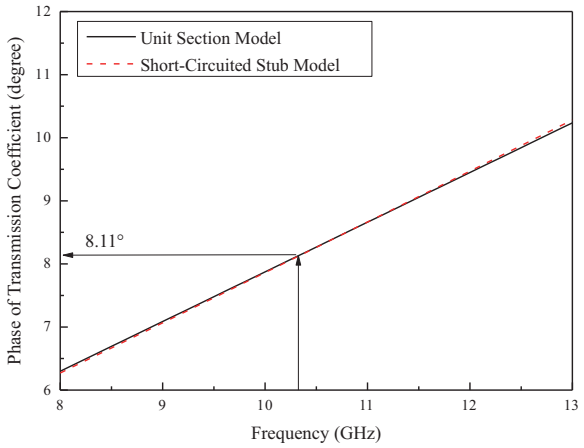

FIGURE 9. Comparison between the phases of the transmission coefficients for the unit section model of Fig. 8(a) and short-circuited stub model of Fig. 8(b).

TABLE 2. Dimensions of the short-circuited stub.

UNIT: mm

L_S	W_S	W_{SP}
0.54	0.15	0.13

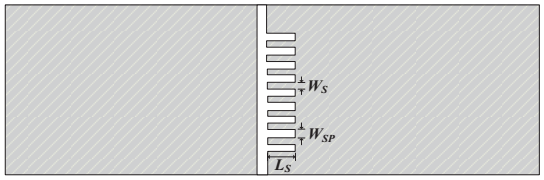

FIGURE 10. Cascade of the short-circuited stubs.

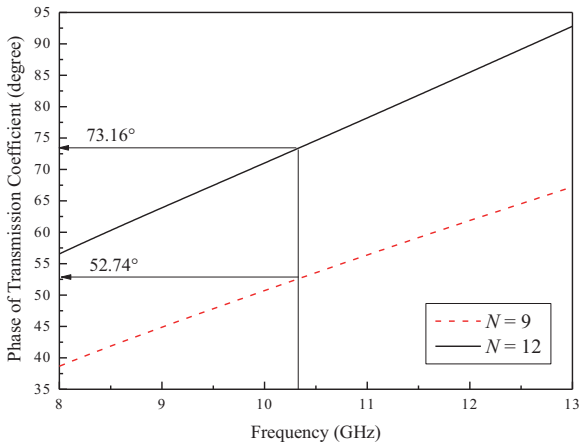

FIGURE 11. Phases of the transmission coefficients for the cascade of the short-circuited stubs.

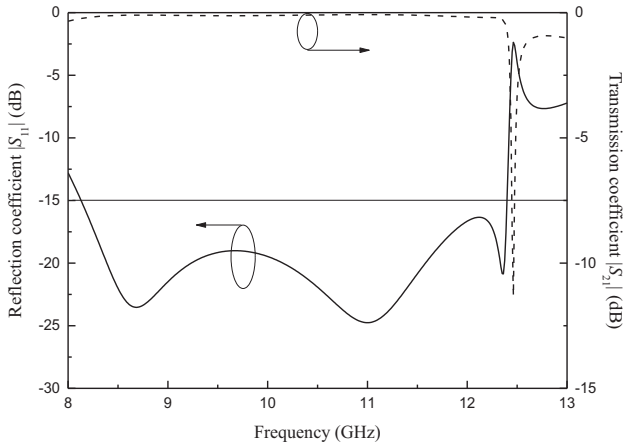

FIGURE 12. The frequency responses of the reflection coefficient $|S_{11}|$ and transmission coefficient $|S_{21}|$ for the miniaturized CPW-to-RWG transition using the resonator with the impedance matching element.

The short-circuited stub model shown in Fig. 8(b) is then implemented with a short-circuited stub and cascaded with $N = 9$ sections as shown in Fig. 10. The dimensions of the short-circuited stub are listed in Table 2. Fig. 10 and the dimensions listed in Table 2 are simulated using the Ansoft HFSS. The frequency response of the phase of the transmission coefficient is shown in Fig. 11. As can be observed from Fig. 11, the phase of the transmission coefficient is only 52.74°, which is much smaller than the expected value of $\theta = 73°$. This phenomenon might be caused by the coupling effect between the adjacent short-circuited stubs, which can be compensated by adding more sections of the short-circuited stubs. By increasing $N = 12$, Fig. 10 is simulated by using the Ansoft HFSS, and the frequency response of the phase of the transmission coefficient is shown in Fig. 11. As can be seen from Fig. 11, the phase of the transmission coefficient is increased to 73.16°, which meets the expected value of $\theta = 73°$.

3.3. Frequency Responses

By replacing the selected part of path A shown in Fig. 1(b) with the cascade of the short-circuited stubs shown in Fig. 10, the miniaturized CPW-to-RWG transition using the resonator with the impedance-matching element can be formed as shown in Fig. 7. The dimensions can be found in Table 1 and Table 2. As seen from Table 1 and Table 2, the overall length of the transition is as small as 5.9 mm. Compared with the CPW-to-RWG transition using the resonator with the impedance-matching element, the length of the transition is further reduced from 7.66 mm to 5.9 mm. Fig. 7 along with the dimensions listed in Table 1 and Table 2 is simulated by using the Ansoft HFSS, and the frequency responses of the reflection and transmission coefficients are shown in Fig. 12. As can be seen from Fig. 12, the frequency range, for which the reflection coefficient is smaller than -15 dB, covers from 8.05 GHz to 12.38 GHz, nearly encompassing the whole X-band (8.2–12.4 GHz), and the corresponding transmission coefficient in this frequency range is larger than -0.22 dB.

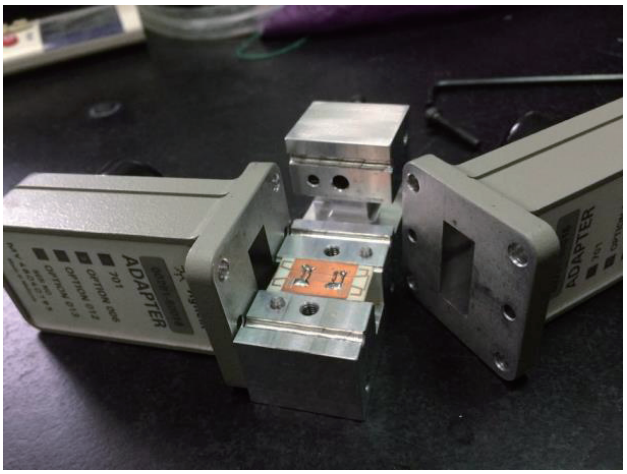

FIGURE 13. Measurement setup for the back-to-back miniaturized CPW-to-RWG transition using the resonator with the impedance matching element.

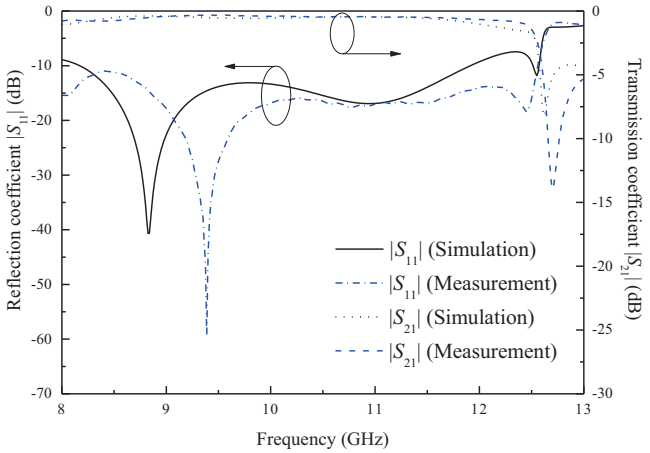

FIGURE 14. Comparison between the simulation and measurement results for the back-to-back miniaturized CPW-to-RWG transition using the resonator with the impedance matching element.

TABLE 3. Performances of some broadband transitions.

Transition Type	15 dB Operation Band (Waveguide Band)	15 dB FBW	Circuit Length Normalized to X-band
Ridged Waveguide [5]	110–170 GHz (D)	42.86%	27.18 mm
Fin-Line Taper [6]	8.2–12.4 GHz (X)	40.78%	15 mm
Slotline Probe [8]	8.2–12.7 GHz (X)	43.06%	13.97 mm
Horizontal Probe [9]	8.2–12.4 GHz (X)	40.78%	12.6 mm
Bow-Tie Antenna [10]	8.5–12.7 GHz (X)	39.62%	12 mm
Stub Resonators [12]	8.3–12.9 GHz (X)	43.40%	7.8 mm
EBG Structure [13]	170–260 GHz (WR4)	41.86%	11.4 mm
Half-Wavelength PS	**8.05–12.18 GHz (X)**	**40.83%**	**7.66 mm**
Short-Circuited Stub PS	**8.05–12.38 GHz (X)**	**42.38%**	**5.9 mm**

3.4. Verification

To verify the simulation results, two miniaturized CPW-to-RWG transitions using a resonator with an impedance-matching element are cascaded and fabricated as shown in Fig. 13. It is then measured by using the Agilent E8363B PNA after the network analyzer is calibrated with the SOLT waveguide components. The measured frequency responses of the reflection and transmission coefficients for the back-to-back transition are shown in Fig. 14 along with the simulated frequency responses of the reflection and transmission coefficients. As demonstrated in Fig. 14, the simulation and measurement results are in reasonable agreement except for some frequency shifts, which may be attributed to the PCB fabrication process.

4. CONCLUSION

This paper proposes a compact and broadband CPW-to-RWG transition using a resonator with an impedance-matching element. By adequately designing the dimensions of the resonator and impedance-matching element, a compact size and broadband response can be achieved at the same time. The frequency range for which the reflection coefficient is less than -15 dB covers from 8.05 GHz to 12.18 GHz (FBW = 40.83%), almost encompassing the whole X-band (8.2–12.4 GHz), and the corresponding transmission coefficient in this frequency range is larger than -0.22 dB. Meanwhile, the size of the transition is as small as 7.66 mm. In order to further reduce the size of the transition, a short-circuited stub phase shifter is used to replace the half-wavelength phase shifter, resulting in a more compact and broadband CPW-to-RWG transition using the resonator with the impedance-matching element. The frequency range for which the reflection coefficient is less than -15 dB covers from 8.05 GHz to 12.38 GHz (FBW = 42.38%), nearly encompassing the whole X-band (8.2–12.4 GHz), and the corresponding transmission coefficient in this frequency range is larger than -0.22 dB. Meanwhile, the transition size is further reduced from 7.66 mm to 5.9 mm. To verify the simulation results, two CPW-to-RWG transitions using a resonator with an impedance-matching element are back-to-back connected, fabricated, and measured. The simulation and measurement results are in reasonable agreement. Table 3 summarizes the perfor-

mances of some broadband transitions. As can be seen from Table 3, the miniaturized CPW-to-RWG transition using the resonator with the impedance-matching element has the smallest size and broadband response.

ACKNOWLEDGEMENT

This work was partly supported by the National Science and Technology Council, Taiwan, under Grant NSTC 112-2221-E-011-087. The authors would like to thank Wireless Communications & Applied Electromagnetic LAB, National Taiwan University of Science and Technology, for providing the simulation environment of Ansoft® HFSS and the measurement instruments.

REFERENCES

[1] Gmitrovic, M. V., B. D. Milovanovic, and Z. D. Milosavljevic, "Fixed and variable slope CATV amplitude equalizers," *Applied Microwave and Wireless*, Vol. 10, 76–85, 1998.

[2] Kampa, J. and K. Petrus, "Microwave amplitude equalizer," in *13th International Conference on Microwaves, Radar and Wireless Communications. MIKON-2000. Conference Proceedings (IEEE Cat. No. 00ex428)*, Vol. 1, 37–40, 2000.

[3] Wang, Y., D. Zhou, Y. Zhang, and C. Chang, "Using multilayered substrate integrated waveguide to design microwave gain equalizer," *Advances in Materials Science and Engineering*, Vol. 30, 1341–1344, 2014.

[4] Tang, S., Y. Zhang, and J. Zhang, "A novel compact size microstrip equalizer based on spiral resonators," in *2010 International Conference on Microwave and Millimeter Wave Technology*, 730–733, 2010.

[5] Wang, Z. and B. Jia, "Research on microwave equalizer of aperture-backed technique," in *2008 8th International Symposium on Antennas, Propagation and EM Theory*, 1375–1378, 2008.

[6] Mellor, D. J., "On the design of matched equalizers of prescribed gain versus frequency profiles," in *1977 IEEE MTT-S International Microwave Symposium Digest*, 308–311, 1977.

[7] Ying, Z., D.-F. Zhou, Z.-X. Niu, and B. Zhao, "A improved branch resonator and it's application in microstrip equalizer designing," in *2007 International Conference on Microwave and Millimeter Wave Technology*, 1–4, 2007.

[8] Ying, Z., D.-F. Zhou, Z.-X. Niu, and D.-W. Zhang, "Study of the influence of resistors for microstrip equalizer," in *2005 Asia-Pacific Microwave Conference Proceedings*, Vol. 5, 4, 2005.

[9] Zhang, Y., M. Yu, B. Yan, and R. Xu, "Research on the millimeter wave power equalizer," in *2007 International Symposium on Microwave, Antenna, Propagation and EMC Technologies for Wireless Communications*, 446–449, 2007.

[10] Zhou, T.-F., Y. Zhang, and R.-M. Xu, "Research on the millimeter wave gain equalizer," in *2011 IEEE International Conference on Microwave Technology & Computational Electromagnetics*, 180–182, 2011.

[11] Gourav, C. and G. Anand, "Non-reflective broadband microwave gain equalizer for EW applications," *2019 IEEE MTT-S International Microwave and RF Conference (IMARC)*, 1–4, 2019.

[12] Jiang, S., J. Xu, and D. Ding, "A 5–19 GHz amplitude-shaped power amplifier using microstrip sirs loaded with film resistors," in *2016 IEEE International Conference on Microwave and Millimeter Wave Technology (ICMMT)*, Vol. 1, 138–140, 2016.

[13] Pozar, D. M., *Microwave Engineering*, John Wiley & Sons, 2011.